JOURNAL OF AIRCRAFT
Vol. 33, No. 3, May–June 1996

Navier–Stokes Computations on Flexible Advanced Transport Wings in Transonic Regime

Guru P. Guruswamy* and Eugene L. Tu†
NASA Ames Research Center, Moffett Field, California 94035-1000

Steady, unsteady, and aeroelastic computations are performed on an advanced transonic wing configuration. The flow is modeled by the Navier–Stokes equations, and structures for aeroelastic computations are modeled by the modal equations. The inadequacy of Euler equations and the importance of using the Navier–Stokes equations with a turbulence model is demonstrated for supercritical flows in the transonic regime. The effect of Mach number on steady pressure distributions is illustrated. Steady flow computations for transonic wings are compared with wind-tunnel data and also with equivalent conventional wings. Unsteady computations are made in the context of demonstrating the use of the indicial approach for generating aerodynamic data for aeroelastic computations. By using the unsteady data generated by indicial responses, a computationally efficient approach of computing preliminary flutter boundaries is demonstrated. The effect of Mach number on the flutter boundary including the prediction of the transonic flutter speed dip is demonstrated. The flutter boundaries of transonic wings are compared with equivalent conventional wings. Characteristics of the flutter boundaries are correlated with aerodynamic flow characteristics.

Introduction

THERE is a continuous effort to improve the performance of subsonic transport aircraft.[1] One attempt is to improve the fuel efficiency by extending the flight regime to high subtransonic Mach numbers to increase lift-to-drag ratios and flight speeds. To avoid the high drag associated with strong shock waves, these advanced transports require modern wing sections such as supercritical wings that delay the shock-wave formation. Early experiments have shown that these advanced wings experience an undesirable reduction in the flutter speed at the transonic regime. Such a phenomenon, commonly known as transonic-dip, is more pronounced for wings with supercritical airfoils.[2] To accurately predict the flutter characteristics, it is necessary to model viscous flows using the Navier–Stokes equations.

To date, advanced wing calculations have been restricted to steady and unsteady computations on rigid wings. However, it is necessary to account for the wing's flexibility to accurately compute its aeroelastic characteristics. The aeroelastic deformation resulting from this flexibility can significantly change the nature of the flow. Strong interactions between the flow and structures can lead to sustained aeroelastic oscillations for swept wings.[3] Also, it is necessary to include the flexibility for proper correlations of computed data with experiments, particularly with those obtained from flight tests. To compute the flows accurately, it is necessary to include both aerodynamic and structural effects of the body. Recent efforts have been made to include the flexibility effects for wing–body configurations.[4] In this work, the flow is modeled using the Navier–Stokes equations and aeroelastic computations are made by using an uncoupled approach.

The computer code, ENSAERO, computes the unsteady aerodynamics and aeroelasticity of aircraft by using the thin-layer Navier–Stokes equations.[5] Previous work has demonstrated the code's capability to compute aeroelastic responses by simultaneously integrating the Navier–Stokes equations and the structural equations of motion, by using aeroelastically adaptive dynamic grids.[4] The flow is solved by time-accurate, finite difference schemes based on the Beam–Warming algorithm with the Baldwin–Lomax turbulence model.

This work studies the transonic aeroelastic characteristics of advanced transports. The AGARD standard, Lockheed–Air Force–NASA–NLR (LANN) wing model,[6] are considered for this study. The computed steady data is validated with the wind-tunnel data. Steady flows are also compared with a model having equivalent conventional airfoil section. Detailed aeroelastic computations are made to predict the transonic dip and results are compared with the equivalent conventional wing. The characteristics of the flutter boundary are related to the aerodynamic flow characteristics.

Governing Aerodynamic Equations

The strong conservation-law form of the thin-layer Navier–Stokes equations is used for shock-capturing purposes. The thin-layer version of the equations in generalized coordinates can be written as[7]

$$\partial_\tau \hat{Q} + \partial_\xi \hat{E} + \partial_\eta \hat{F} + \partial_\zeta \hat{G} = Re^{-1}\partial_\zeta \hat{S} \qquad (1)$$

where $\hat{Q}$, $\hat{E}$, $\hat{F}$, $\hat{G}$, and $\hat{S}$ are flux vectors in generalized coordinates. The following transformations are used in deriving Eq. (1):

$$\tau = t, \quad \xi = \xi(x, y, z, t), \quad \eta = \eta(x, y, z, t), \quad \zeta = \zeta(x, y, z, t)$$

It should be emphasized that the thin-layer approximation is valid only for high Reynolds number flows, and very large turbulent eddy viscosities invalidate the model.

To solve Eq. (1), ENSAERO has time-accurate methods based on both central difference[8] and upwind schemes.[9] In this work the diagonal form of the Beam–Warming central difference scheme is used.

Presented as Paper 94-1725 at the AIAA Dynamic Specialists Conference, Hilton Head, SC, April 21–22, 1994; received May 15, 1994; revision received Sept. 1, 1995; accepted for publication Dec. 5, 1995.

*Research Scientist, Computational Aerosciences Branch. Associate Fellow AIAA.

†Research Scientist, Computational Aerosciences Branch. Member AIAA.

Aeroelastic Equations of Motion

The governing aeroelastic equations of motion are obtained by using the Rayleigh–Ritz method. In this method, the resulting aeroelastic displacements at any time are expressed as a function of a finite set of assumed modes. The contribution of each assumed mode to the total motion is derived by Lagrange's equation. Furthermore, it is assumed that the deformation of the continuous wing structure can be represented by deflections at a set of discrete points. This assumption facilitates the use of discrete structural data, such as the modal vector, the modal stiffness matrix, and the modal mass matrix. These can be generated from a finite element analysis or from experimental influence coefficient measurements. In this study, the finite element method is employed to obtain the modal data.

It is assumed that the deformed shape of the wing can be represented by a set of discrete displacements at selected nodes. From the modal analysis, the displacement vector $\{d\}$ can be expressed as

$$\{d\} = [\phi]\{q\} \tag{2}$$

where $[\phi]$ is the modal matrix.

The final matrix form of the aeroelastic equations of motion is

$$[M]\{\ddot{q}\} + [G]\{\dot{q}\} + [K]\{q\} = \{Z\} \tag{3}$$

where $[M]$, $[G]$, and $[K]$ are modal mass, damping, and stiffness matrices, respectively. The modal aerodynamic force vector is $\{Z\}$.

With the previous modal equations of motion, flutter boundaries can be computed by using coupled and uncoupled approaches.[10] Coupled approaches require direct time integration of flow and structural equations. This approach is accurate for flows with high nonlinearities, however, it is computationally expensive. On the other hand, the uncoupled approach that is computationally less expensive requires an additional assumption that the aerodynamic data can be linearly superimposed among modes. As demonstrated in Refs. 10 and 11 earlier, and more recently in Ref. 12, the uncoupled method can be an effective approach to predict the preliminary flutter characteristics required in the early stages of design. Based on the flutter computations of airfoils in Ref. 10, the uncoupled approach requires one-tenth of the computational effort required for the coupled analysis. In this work, the uncoupled approach is used to compute the flutter boundary.

The uncoupled approach assumes that the wing will be undergoing simple harmonic motion so that the generalized coordinates $\{q\}$ take the form

$$\{q\} = \{\bar{q}\}e^{i\omega t} \tag{4}$$

where ω is the frequency of oscillation at flutter. Substituting Eq. (4) in Eq. (3) and introducing the concept of artificial damping,[13] Eq. (3) can be represented as a complex eigenvalue equation given by

$$[K]^{-1}[[M] - C[Q]]\{\bar{q}\} = \lambda\{\bar{q}\} \tag{5}$$

where generalized modal force $Q_{ij} = (1/S)\int\int \Delta C_{pj} h_i \, dx \, dy$; i and j represent modes. $C = 2\rho b^2 S/k^2$, where $k = \omega c/U$, U being the flight speed; h = modal displacement; S = surface area of the wing; and $\lambda = (1 + ig)/\omega^2$, complex eigenvalue.

In this work, the standard $U-g$ method[13] is used to compute the flutter boundary. In the $U-g$ method, modal aerodynamic force matrix $[Q]$ is required as a function of frequency for each selected mode. One way to generate the data for nonlinear flows is to compute unsteady aerodynamic data at a set of preselected frequencies and then interpolating the data for required frequencies in the $U-g$ method. Typically, data at 3–4 frequencies are required to make a reasonable prediction of the flutter boundary. The computation of data has to be repeated for all selected modes. Repeating computations for each frequency can be avoided by using the indicial approach.[14] In this approach, data for all frequencies can be extracted from a single unsteady response computation. The indicial approach requires an assumption that the unsteady flow can be linearized about a nonlinear steady flow. Such an assumption is valid for a small perturbation. Classical flutter starts as a small perturbation phenomenon, and it is therefore appropriate to use the indicial approach to make a preliminary prediction of the flutter boundary. In this work, the unsteady data required for the $U-g$ approach are computed using the indicial approach.

Results

Steady Flow Computations on LANN Wing Model

To demonstrate the need of using the Navier–Stokes equations for supercritical wings, steady computations are made for the LANN supercritical wing model. Note that an earlier study to compute flows over this model has been performed,[15] and it showed that the inviscid potential equations are not entirely adequate to resolve the details of the flow. Furthermore, results given in this section will show that the Euler equation also does not provide adequate prediction.

The LANN model has an aspect ratio of 7.92, a taper ratio of 0.40, and a leading-edge sweep angle of 27.5 deg. The airfoil sections are supercritical with a constant thickness-to-chord ratio of 12%. This model was tested in the transonic wind tunnel (HST) of the National Aerospace Laboratory (NLR), The Netherlands. Details of steady flow measurements are given in Ref. 6.

Computations are made using the built-in C-H grid topology available in the wing version of ENSAERO. A grid refinement study is conducted to select a grid. The default grid of size 151 × 35 × 35 (151 points in streamwise direction, 35 points in spanwise direction, and 35 points in surface-normal direction), most commonly used in ENSAERO for wing calculations and a finer grid of size 191 × 35 × 35, are selected. For both grids there are 24 spanwise sections on the wing surface. The finer grid has 960 more grid points on the wing surface than the default grid. Steady flow computations are made at M = 0.87- and 3.0-deg angle of attack (AOA). The surface pressures from the default grid agrees well with those from the fine grid for all sections. Results are illustrated for the 47.5% semispan section in Fig. 1. From this it is concluded that the 151 × 35 × 35 grid is adequate for the rest of the calculations.

Results for M = 0.87 and AOA = 3.0 deg are compared with the wind-tunnel measurements. Figure 2 compares the computed and measured pressures for the 47.5% semispan section. There are minor differences near 50% chord that are within the error limits of both the experiment and the computation. Comparisons are also good at all other sections. Euler com-

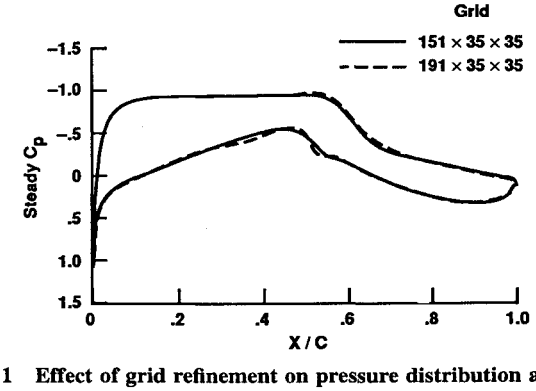

Fig. 1 Effect of grid refinement on pressure distribution at M = 0.87 and α = 3 deg for 47.5% section.

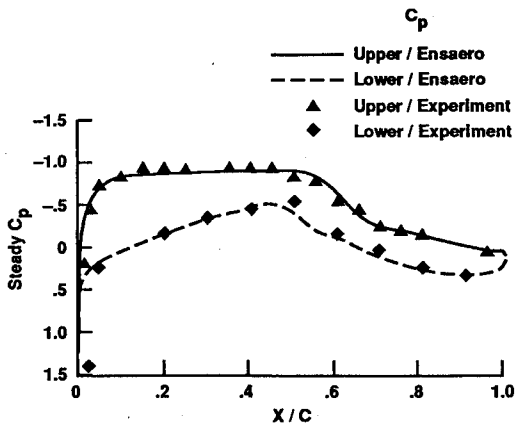

Fig. 2 Comparison between computed and measured pressure distributions at $M = 0.87$ and $\alpha = 3$ deg for 47.5% section.

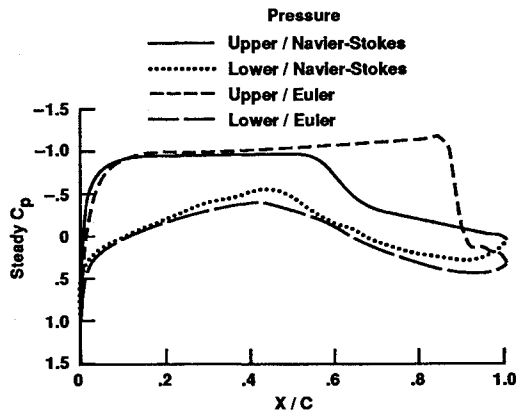

Fig. 3 Comparison between pressure distributions from the Euler and Navier–Stokes equations at $M = 0.87$ and $\alpha = 3$ deg for 47.5% section.

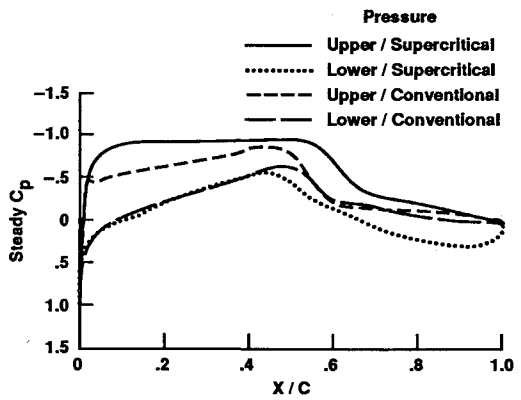

Fig. 4 Comparison between pressure distributions for supercritical and conventional wings at $M = 0.87$ and $\alpha = 3$ deg for 47.5% section.

putations were made to study the effect of viscosity for this case. Results from the Euler equations are compared with those from the Navier–Stokes equations in Fig. 3. The Euler equation gives a stronger shock wave that is located further downstream than the actual shock wave. This result demonstrates that it is important to account for the viscous effects using the Navier–Stokes equations for supercritical wings, even at moderate flow conditions.

One of the objectives of this work is to compare flow and aeroelastic characteristics of supercritical wings with equivalent conventional wings. This article considers a conventional

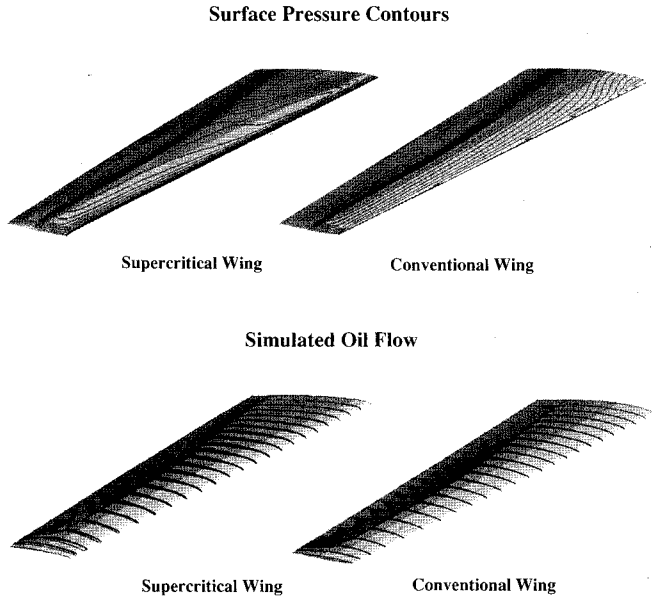

Fig. 5 Comparison of surface flow characteristics between supercritical and conventional wings at $M = 0.87$ and $\alpha = 3$ deg.

wing with NACA 64A012 airfoil sections that has the same planform and thickness ratio as the LANN wing. Figure 4 shows the comparison of steady pressures between LANN and conventional wings for the 47.5% semispan. As expected, the supercritical wing has higher lift than the conventional wing. The additional lift comes from lower negative pressures on the upper surface and higher positive pressures near the trailing-edge lower surface because of aft-loading. The LANN wing gives about 30% more total lift than the conventional wing. Upper surface pressure contours and simulated oil flow patterns are given for both wings in Fig. 5. Figures 4 and 5 illustrate a stronger transonic shock wave located further downstream for the LANN (supercritical) wing. Effects of these and other aerodynamic characteristics on the flutter boundary will be illustrated in the following section.

Aeroelastic Computation on LANN Wing Model

One of the main purposes of this work is to study the aeroelastic characteristics of advanced transonic wings. For this purpose, the original LANN wing that was designed as a pressure model is modified to an aeroelastic model by representing the wing structure by a uniform plate of 0.1 in. thickness. The wing root length is the same 14.2 in. as the original wind-tunnel rigid model. The first bending ω_{h1}, first torsional $\omega_{\alpha 1}$, second bending ω_{h2}, and second torsional $\omega_{\alpha 2}$ frequencies of this model are 2.98, 15.68, 37.0, and 48.68 Hz, respectively. These frequencies represent structural properties of a typical transport wing. Computations are made for Mach numbers ranging from 0.60 to 0.85 in increments of 0.025 at an AOA of 3.0 deg.

As stated earlier, the flutter boundaries are computed using the U–g method with the required unsteady data generated from the indicial method. In this work, indicial responses of sectional lifts and moments are computed for the rigid wing by giving a step change in the AOA. These indicial responses are used to compute the generalized modal forces required for the U–g approach. The validity of using the indicial approach is verified by computing the unsteady aerodynamic data both by time-integration and indicial approach at $M = 0.80$ and AOA = 3.0 deg.

For time integration, unsteady data are obtained by integrating the aerodynamic equations when the wing is oscillating in pitch motion about an axis located at the 50% root chord. Indicial responses are obtained by giving a step change in pitching AOA of 0.1 deg. Figure 6 shows the magnitude of

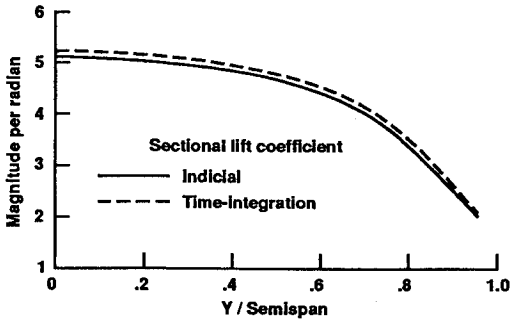

Fig. 6 Comparison of magnitude of sectional lifts between indicial and time integration method for $M = 0.80$, $\alpha = 3$ deg, and $k = 0.30$.

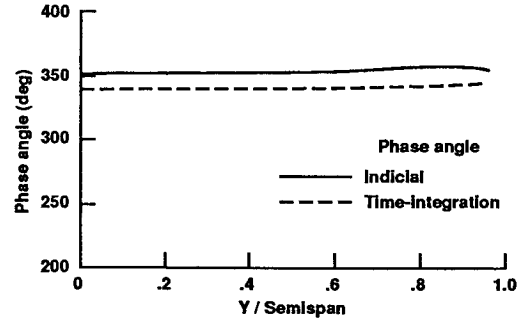

Fig. 7 Comparison of phase angles of sectional lifts between indicial and time integration method for $M = 0.80$, $\alpha = 3$ deg, and $k = 0.30$.

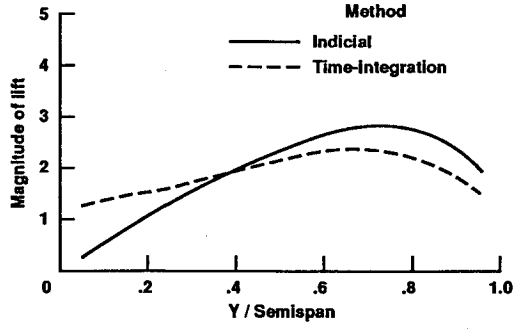

Fig. 8 Comparison of magnitude of sectional lifts between indicial method for rigid wing and time integration method for flexible wing at $M = 0.80$, $\alpha = 3$ deg, and $k = 0.30$.

sectional lifts computed from both methods for a reduced frequency $k = 0.30$. About 5000 time steps are required for the indicial response to reach a steady-state condition with a computational time step size of 0.00325. The total CPU time required for the indicial response, including the time required for the steady-state initial solution, is about 2.5 h on a single Cray C-90 processor. This is based on the fact that ENSAERO runs at about 400 Mflops and requires about 7 μs/time step/grid point. The time-integration method required three cycles with 3600 time steps per cycle (the computational step size is equal to 0.00725) for complete calculation. This computation required about 4.5 CPU hours. Figure 6 shows that throughout the span, the indicial lift is about 2% less than the time-integration lift. This result shows a good agreement between the methods. The corresponding phase angles are plotted in Fig. 7, which also shows a good agreement throughout the wingspan. These results demonstrate that the indicial approach is adequate to compute the unsteady aerodynamic data.

Since the indicial data are computed on a rigid wing, an additional assumption that the sectional forces depend mainly on the local sectional displacements is required to extend the indicial data to flexible modes. Again, this assumption is valid for small perturbations. This is validated by comparing the unsteady data computed by the indicial approach on a rigid wing with that computed by time integration on a flexible wing. Both wings were oscillated in their first torsional modes at $M = 0.80$ and AOA = 0.0 deg. Figure 8 compares the magnitude of sectional lifts between the indicial and time-integration method. The lift values for each section are scaled with respect to the tip AOA of 1 deg. Both curves show the same trend. Inboard of 40% semispan, the indicial approach predicts higher lift than that from the time-integration approach. Outboard of 40% semispan, the trend is opposite. Phase angles compare favorably between the two methods.

Steady-state solutions are computed on the rigid wing for Mach numbers from 0.60 to 0.85 in increments of 0.025, which are required as starting solutions for computing the indicial responses. Figure 9 shows the plots of upper surface pressures at 50% semispan station for the LANN wing. The shock wave starts developing at about $M = 0.75$, and grows stronger with an increase in Mach number. As M reaches 0.85, the flow starts separating behind the shock wave. Figure 10 shows similar plots for the conventional wing. For this case, the shock wave starts developing at $M = 0.80$. The influence

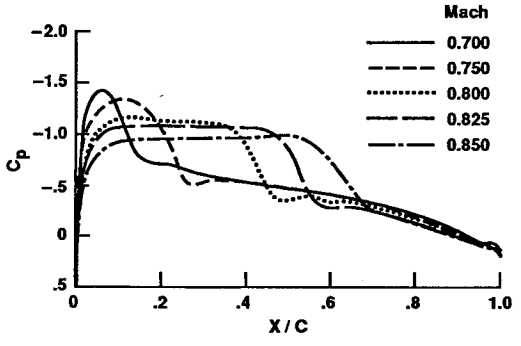

Fig. 9 Effect of Mach number on pressure distributions at 47.5% section for supercritical wing at $\alpha = 3$ deg.

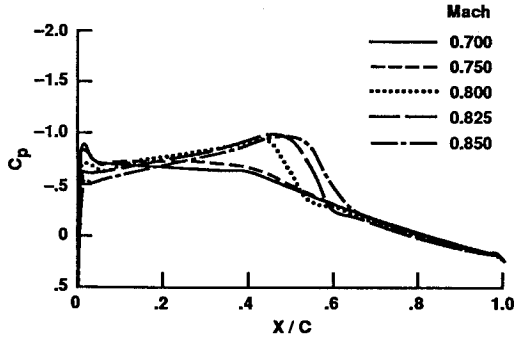

Fig. 10 Effect of Mach number on pressure distributions at 47.5% section for conventional wing at $\alpha = 3$ deg.

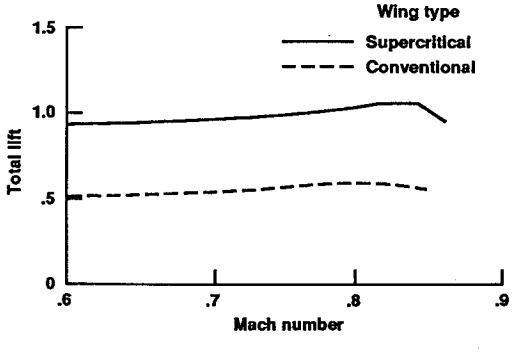

Fig. 11 Comparison of total lift vs Mach number plots between supercritical and conventional wings for $\alpha = 3$ deg.

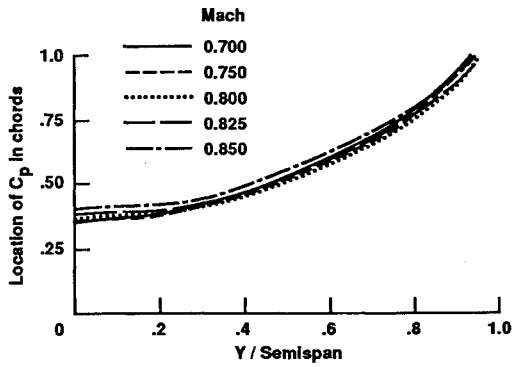

Fig. 12 Effect of Mach number on CP distributions for supercritical wing at α = 3 deg.

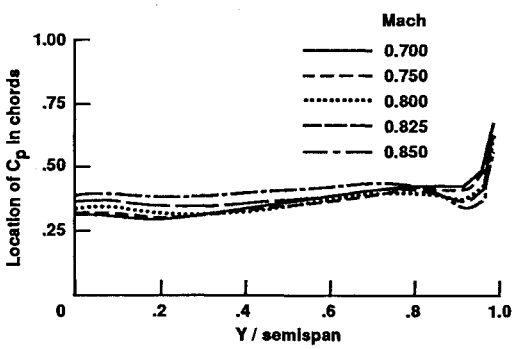

Fig. 13 Effect of Mach number on CP distributions for conventional wing at α = 3 deg.

of Mach number on total lift is shown for both wings in Fig. 11. Rate of increase in the lift starts falling for the conventional wing at M = 0.825, slightly before it occurs for the LANN wing at about M = 0.84. The effects of Mach number on center of pressures (CP) are shown in Figs. 12 and 13 for the LANN and conventional wings, respectively. For the LANN wing, inboard of 40% semispan, the CP line is behind the elastic axis located at the 50% chord. Outboard of 40% semispan, the CP line is in front of the elastic axis. For the conventional wing, most of the CP line is located behind the wing elastic axis, except near the tip section. For both wings, the CP line moves aft with increasing Mach number. For the LANN wing, the location of the CP line is slightly less sensitive to Mach number than that for the conventional wing.

Indicial responses are computed for all Mach numbers starting from the converged steady-state solutions. Flutter speeds are computed by using the $U-g$ method based on the unsteady aerodynamic data obtained from the indicial method. Note that before using the data from the indicial approach, the validity of the unsteady data should be verified against the time-integration method by making comparisons similar to those shown in Figs. 6 and 8. Since the indicial results shown in Fig. 8 for the flexible case are less favorable than for the rigid case (shown in Fig. 6), the following flutter computations are limited to small perturbations. However, the flutter boundaries generated can be valuable for preliminary design and give good initial conditions required for time-integration methods, which can further improve the accuracy of results.

Figure 14 shows a plot of flutter speed $\bar{U}$ ($=2U/c\omega_{\alpha 1}$ where U is the flutter speed) vs Mach number for both wings. Flutter speeds are lower for the LANN wing than for the conventional wing. For the LANN wing the transonic dip occurs at about M = 0.775. In Ref. 16 an analysis was made to relate the flutter boundary behavior to the basic flow characteristics. Based on two-dimensional airfoil calculations in Ref. 16, it is observed that the flutter speed decreases with increase in lift. Similar behavior is also observed by comparing Figs. 14 and 11. In

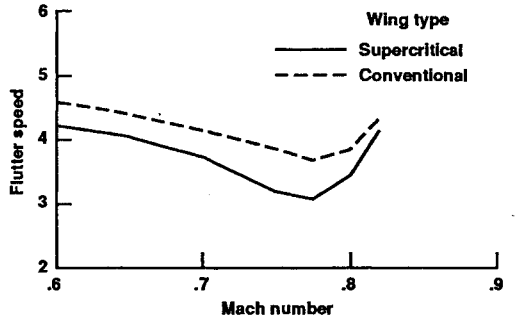

Fig. 14 Comparison of flutter boundaries between supercritical and conventional wings at α = 3 deg.

Ref. 16 it was also observed that the flutter speed increases as the CP line moves towards the elastic axis. Since a part of the CP line inboard of 40% semispan moves towards the elastic axis, and the rest moves away from the elastic axis, there is more influence of lift than the CP line on the flutter curve for the LANN wing. As a result, there is a sharper drop in the flutter speed. However, as the lift starts leveling off near peak lift, the flutter speed starts increasing. Similar behavior is also observed for the conventional wing. However, this wing has a less sharper dip since most of the CP line moves towards the elastic axis. Therefore, there is a continuous compensating effect of lift and CP line location on the flutter curve. The dip that occurs near M = 0.775 is less severe than that for the LANN wing. These observations agree with those made in Ref. 2 based on wind-tunnel measurements.

Conclusions

Detailed aerodynamic and aeroelastic computations are made for transonic wing configurations. The use of indicial response data in predicting preliminary flutter characteristics is demonstrated by using an uncoupled approach. Each flutter point required a computational time about three times that of steady flow computations. This is considerably less, by almost a factor of 10, than the time-integration method used in the coupled approach. Note that the present approach is valid only for small unsteady perturbations about a nonlinear steady-state solution. Since flutter starts as a small perturbation phenomenon, the present approach is computationally efficient to predict preliminary flutter characteristics.

The flutter and aerodynamic characteristics of transonic wings are compared with conventional wings. For both wings, it is found that the trend of the flutter curve is indirectly related to the flow characteristics such as lift and center of pressures. The dip in the flutter curves are successfully predicted for both wings, and they are correlated with the basic flow characteristics.

Most of the current computations are limited to wing models with assumed structural properties. Further computations using realistic structural data will be made for the wing–body configurations.

References

[1]Goldhammer, M. I., and Steinle, F. W., "Design and Validation of Advanced Transonic Wings Using CFD and Very High Reynolds Number Wind Tunnel Testing," International Council of the Aeronautical Sciences 90-2.6.2, 17th Congress, Stockholm, Sweden, Sept. 1990.

[2]Farmer, M. G., Hanson, P. W., and Wynne, E. C., "Comparison of Supercritical and Conventional Flutter Characteristics," NASA TM X-72837, May 1976.

[3]Guruswamy, G. P., "Vortical Flow Computations on a Flexible Blended Wing-Body Configuration," *AIAA Journal*, Vol. 30, No. 10, 1992, pp. 2497–2503.

[4]Guruswamy, G. P., and Byun, C., "Fluid-Structural Interactions Using Navier-Stokes Flow Equations Coupled with Finite Element Structures," AIAA Paper 93-3087, July 1993.

[5]Guruswamy, G. P., "ENSAERO—A Multidisciplinary Program

for Fluid/Structural Interaction Studies of Aerospace Vehicles," *Computing Systems in Engineering*, Vol. 1, Nos. 2–4, 1990, pp. 237–256.

[6]Horsten, J. J., Den Boer, R. G., and Zwaan, R. J., "Unsteady Transonic Pressure Measurements on a Semispan Wind Tunnel Model of a Transport-Type Supercritical Wing, Part I General Description, Aerodynamic Coefficients and Vibration Modes," Air Force Wright Aeronautical Labs. TR-83-3039, Dayton, OH, April 1982.

[7]Peyret, R., and Viviand, H., "Computation of Viscous Compressible Flows Based on Navier-Stokes Equations," AGARD AG-212, Sept. 1975.

[8]Beam, R., and Warming, R. F., "An Implicit Finite-Difference Algorithm for Hyperbolic Systems in Conservation Law Form," *Journal of Computational Physics*, Vol. 22, No. 9, 1976, pp. 87–110.

[9]Obayashi, S., Guruswamy, G. P., and Goorjian, P. M., "Streamwise Upwind Algorithm for Computing Unsteady Transonic Flows Past Oscillating Wings," *AIAA Journal*, Vol. 29, No. 10, 1991, pp. 1668–1677.

[10]Guruswamy, P., and Yang, T. Y., "Aeroelastic Time Response Analysis of Thin Airfoils by Transonic Code LTRAN2," *Computers and Fluids*, Vol. 9, No. 4, 1980, pp. 409–425.

[11]Guruswamy, P., and Goorjian, P. M., "Computations and Aeroelastic Applications of Unsteady Transonic Aerodynamics About Wings," *Journal of Aircraft*, Vol. 21, No. 1, 1984, pp. 37–43.

[12]Lee-Rausch, E. L., and Batina, J. T., "Calculation of AGARD Wing 445.6 Flutter Using Navier-Stokes Aerodynamics," AIAA Paper 93-3476, Aug. 1993.

[13]Fung, Y. C., *Section 6.11, An Introduction to the Theory of Aeroelasticity*, Dover, New York, 1965.

[14]Ballhaus, W. F., and Goorjian, P. M., "Computation of Unsteady Transonic Flow by Indicial Method," *AIAA Journal*, Vol. 16, No. 2, 1978, pp. 117–124.

[15]Malone, J. B., and Ruo, S. Y., "LANN Wing Test Program: Acquisition and Application of Unsteady Transonic Data for Evaluation of Three-Dimensional Computational Methods," Air Force Wright Aeronautical Labs. TR-83-3006, Dayton, OH, Feb. 1983.

[16]Yang, T. Y., Guruswamy, G. P., Striz, A. G., and Olsen, J. J., "Reply by Authors to H. P. Y. Hitch," *Journal of Aircraft*, Vol. 18, No. 2, 1981, pp. 159, 160.